Photochemical & Photobiological Sciences (2022) 21:1637–1645
https://doi.org/10.1007/s43630-022-00247-7

ORIGINAL PAPERS

Ibuprofen molecular aggregation by direct back-face transmission steady-state fluorescence

Paula Y. Steinberg[1] · Nicolás I. Krimer[1] · Gabriela P. Sarmiento[1] · Darío Rodrigues[1,2] · Cristián Huck-Iriart[3] · Daniel Clemens[4] · Andrés Zelcer[5] · Martín Mirenda[1]

Received: 4 February 2022 / Accepted: 12 May 2022 / Published online: 4 June 2022

Abstract

Direct back-face transmission steady-state fluorescence was successfully applied to the study of aggregation of ibuprofen and ibuprofenate anion in solution taking advantage of its own fluorescence. The analysis of the experimental data involves the use of the differential reabsorption model to account for re-absorption phenomenon and the closed association model to describe aggregation. The fluorescence quantum yield of ibuprofenate increases when it aggregates in the presence of sodium, but it markedly decreases when 1-butyl-3-methylimidazolium is used as counterion. The proposed methodology allows the accurate determination of the critical aggregation concentrations and the mean aggregation numbers. Results were supported by complementary techniques such as time-resolved fluorescence, ^{1}H-NMR and small-angle neutron and X-ray scattering. The developed technique constitutes a promising strategy to characterize the aggregation of poorly fluorescent surfactants that aggregates at high concentrations and hence at high absorbance values, conditions in which the most common right-angle configuration for fluorescence acquisition is troublesome due to re-absorption.

Graphical abstract

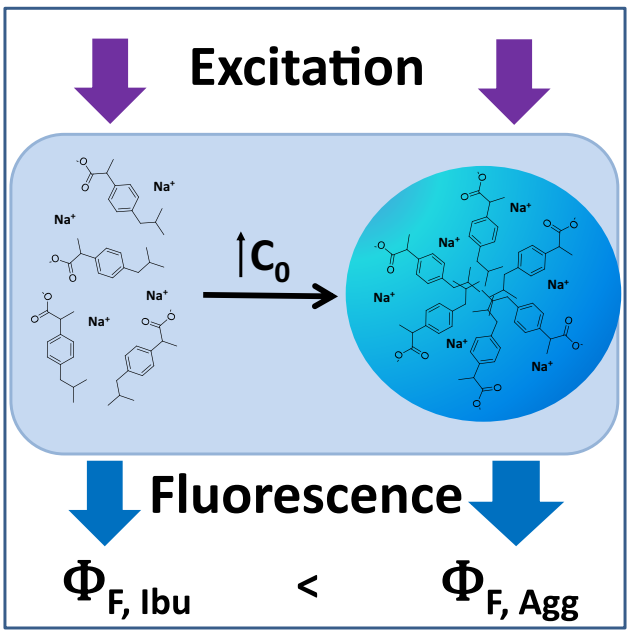

Keywords Ibuprofen · Fluorescence quantum yield · Amphipathic molecules · Aggregation

Extended author information available on the last page of the article

1 Introduction

At present, several experimental methods are available to characterize molecular aggregation processes of amphiphilic molecules in solution. Without being exhaustive, the list includes the measurement of the surface tension [1] and the specific conductivity [2] of the surfactant solutions, and the acquisition of the absorption [3] and the emission [4] spectra of some external probes, to cite only a few. The changes in these properties as the concentration increases serve to determine several aggregation parameters of interest such as the critical micelle concentration (CMC) and the aggregation number (n), whose relevance has been already addressed in many publications [5–8].

Perhaps, one of the most extended methods to determine CMC is the one related to changes in the fluorescence spectrum of pyrene, an external probe that is normally added to the systems to be examined [9]. The ratio between the intensities of the first and the third vibrational bands of the dye (I_1/I_3) varies when the probe is exposed to different polarities. As such, a plot of I_1/I_3 as a function of the surfactant concentration yields sigmoidal-shaped curves that serve to determine CMC by means of different strategies, depending on the ionic or the non-ionic nature of the amphipathic compounds [10]. On the other hand, the fluorescence quenching of an external probe caused by an added external quencher represents another technique used to determine n [11]. In this case, the dye and the quencher are assumed to be located inside the aggregate entities, so the observed quenching can be properly described by Poisson statistics. Within this context, the most extended fluorescence techniques used to determine CMC and n require external probes which can eventually modify the composition of the systems and hence the aggregation parameters to be determined.

In this work, an alternative non-destructive and non-invasive methodology is presented to study the aggregation of fluorescent amphiphilic molecules in solution. The proposed approach is based on the measurement of the steady-state fluorescence of the surfactant molecules in transmission geometry by using a short optical path length. In this case, the fluorescence signal is obtained from the amphipathic fluorescent compound of interest without the addition of any external probe. To assess its relevance, the proposed methodology was implemented in the study of ibuprofen (HIbu) in ethanolic solution and sodium ibuprofenate (NaIbu) and 1-butyl-3-methylimidazolium ibuprofenate (BMimIbu) in water. HIbu is a non-steroidal anti-inflammatory drug and is perhaps the most widely used for treating pain, fever, and inflammation. Its sodium salt NaIbu was recently proposed as a component in nebulizable solutions for an experimental treatment of SARS-CoV-2 disease [12], giving its amphipathic characteristics that favor its insertion into the bilayer membranes of some pathogens. The ibuprofenate anion (Ibu^-) constitutes a poor amphiphilic molecule because its aggregation generally occurs in water in a gradual form at high concentrations—and consequently at high UV–Vis absorbance values—compared with common commercial surfactants. The aggregation behavior of this entity represents a clear example of systems that, at the moment, present serious difficulties to be studied by means of direct fluorescence experiments acquired in a conventional 90º configuration between the excitation and the detection due to the presence of re-absorption.

1.1 Experimental section

1.1.1 Reagents

Ibuprofen (HIbu, microcrystalline powder, purity 99.6%) was purchased from Parafarm® and used as received. Sodium ibuprofenate (NaIbu) was obtained by adding a 1 M aqueous solution of sodium hydroxide to a solution of HIbu in hot acetone. The mixture was cooled and filtered, to obtain a white crystalline product. BMimIbu was synthesized as previously reported [13]. 4-Toluenesulfonic acid (HTos) monohydrate (Sigma-Aldrich, purity > 98.5%) was used as received in water solution as reference for fluorescence quantum yield calculation.

1.1.2 Absorption

Absorption spectra were acquired in a Cary 50 Conc UV–Vis spectrophotometer (Varian), equipped with a thermostated sample holder. The bandwidth of the excitation slit was 1.5 nm. Depending on the optical density of samples, quartz cells of different optical path lengths were used. A 1.0 cm optical path length was used to determine the absorbance of diluted samples to calculate fluorescence quantum yields. The more concentrated samples were measured using a 0.2 cm optical path length. All measurements were performed at 20.0 ± 0.1 °C.

1.1.3 Steady-state emission

Steady-state fluorescence spectra were recorded in a PTI QuantaMaster 4 CW fluorometer, equipped with a xenon short-arc lamp UXL-75XE and a thermostated sample holder. Both excitation and emission monochromators have gratings of 1200 line/mm, in which 1 mm corresponds to a bandwidth of 4 nm. The excitation and emission slits were adjusted in all experiments to 0.375 mm, which is equivalent to a bandwidth of 1.5 nm. The use of the same bandwidth in the absorption and the emission experiments avoids distortions in the Lambert – Beer law. Diluted samples were measured in right-angle configuration using a quartz cell of 1 cm

optical path length. Concentrated highly absorbing samples were measured in transmission geometry using quartz cells of 0.2 cm optical path length to minimize inner-filter effects. The commercial spectrofluorometer was adapted to a transmission configuration in which the fluorescence was collected at 180° with respect to the excitation beam. An Asahi™ SP260 filter was interposed between the excitation source and the samples to minimize any spurious excitation light of higher wavelengths from reaching the sample. The blank was subtracted in each spectrum, and the experimental data were properly corrected using the emission correction function provided by the manufacturer. The observed fluorescence quantum yields were determined at 20.0 ± 0.1 °C relative to a reference, according to the following expression:

$$\Phi_{F,obs}(C) = \Phi_{F,obs}(C_0)\frac{f_x(\lambda_0, C_0)}{f_x(\lambda_0, C)} \cdot \frac{\int_\lambda L_{p,obs}(\lambda_0, \lambda, C)\,d\lambda}{\int_\lambda L_{p,obs}(\lambda_0, \lambda, C_0)\,d\lambda} \quad (1)$$

where $L_{p,\,obs}$ is the experimental observed fluorescence spectra and $f_x(\lambda_0, C)$ and $f_x(\lambda_0, C_0)$ are the absorption factors at the excitation wavelength for a sample of concentration C and for a diluted sample used as reference, respectively. A $\Phi_{F,obs}$ value of 0.20 ± 0.02 was obtained for NaIbu in diluted conditions by using a 1.5×10^{-4} M aqueous solution of HTos in water as reference ($\Phi_{F,HTos} = 0.055 \pm 0.015$) [14].

1.1.4 Time-resolved emission

Time-resolved fluorescence decays were recorded in a HORIBA QM-8075 TCSPC fluorometer, equipped with a pulsed UV LED 260 nm (DeltaDiode-260) and a thermostated sample holder. Samples were measured in right-angle configuration using quartz cells of 0.2 cm optical path length.

1.1.5 NMR

^{1}H-NMR spectra were acquired in a Bruker Avance NEO 500 spectrometer. D_2O was used as solvent.

1.1.6 Small-angle neutron scattering (SANS)

SANS measurements were performed at the time-of-flight V16 instrument at the BER-II reactor located in the Helmholtz-Zentrum Berlin (HZB, Germany). Sample-to-detector distances were 1.7 m and 11.2 m, and a polychromatic beam of cold neutron (wavelength 1.78–3.75 Å and 1.56–9.22 Å, respectively) was used covering a q-range from 0.005 to 0.5 $Å^{-1}$. Sample aperture was 10 mm diameter. Quartz cuvettes (Hellma Analytics) of 1 mm optical path length were used as sample holders. Temperature was kept at 25 °C during measurements. Scattering data was corrected for sample transmission, background and empty cuvette, and intensity was normalized using a H_2O standard. To obtain the 1D scattering intensity, $I(q)$, integration in the range of the momentum transfer q was made, where $q = 4\pi/\lambda \sin(\theta)$ and 2θ is the scattering angle.

1.1.7 Small-angle X-ray scattering (SAXS)

SAXS measurements were carried out using a XEUSS 2.0 (from XENOCS, France) instrument at Laboratorio de Cristalografía Aplicada (Argentina). 2D scattering patterns were registered with a 2D photon counting pixel X-ray detector Pilatus 200 k (DECTRIS, Switzerland). Sample-to-detector distance was 540 mm, incident X-ray beam wavelength was $\lambda = 1.5419$ Å (Cu–K$\alpha_{1,2}$ emission source), and beam size at the sample was 1000×1000 μm^2. Sample holders suitable for liquids at room temperature were used and measures were made in transmission mode. SAXS patterns were acquired for 150 min. 1D reduced data, $I(q)$, was obtained by 360° radial integration of the 2D scattering corrected patterns. Since beam size at the sample was small, smearing effects were not taken into account.

2 Results and discussion

2.1 Ibuprofen in ethanolic solution

Figure 1a shows a schematic representation of the optical arrangement achieved in a commercial spectrofluorometer to acquire the fluorescence signal. The convergence lenses and the short optical path-length of 2 mm are both necessary conditions to attain small irradiation and collection volumes in order to minimize re-absorption and re-emission effects [15]. Convenient short pass or band pass filters must be placed between the excitation monochromator and the sample holder to avoid that spurious light of large wavelengths reaches the sample.

The normalized absorption and emission spectra of a 7×10^{-3} M ethanolic HIbu solution are presented in Fig. 1b. It is observed an overlap between the red side of the absorption spectrum and the blue side of the emission spectrum that may cause re-absorption when the concentration—and hence the absorbance—increases [16]. Indeed, the observed fluorescence quantum yield relative to diluted conditions, $\Phi_{F,obs}/\Phi^0_{F,obs}$, shows a decrease as the concentration increases from 7×10^{-3} M to 0.3 M as depicted in Fig. 1c. The calculated fluorescence quantum yield using the Differential Reabsorption Model, $\Phi_{F,DRM}$ [15], (see section a in the SM for details) shows a similar trend to the experimental ones in the entire concentration range, indicating that the observed behavior can be accurately described by the

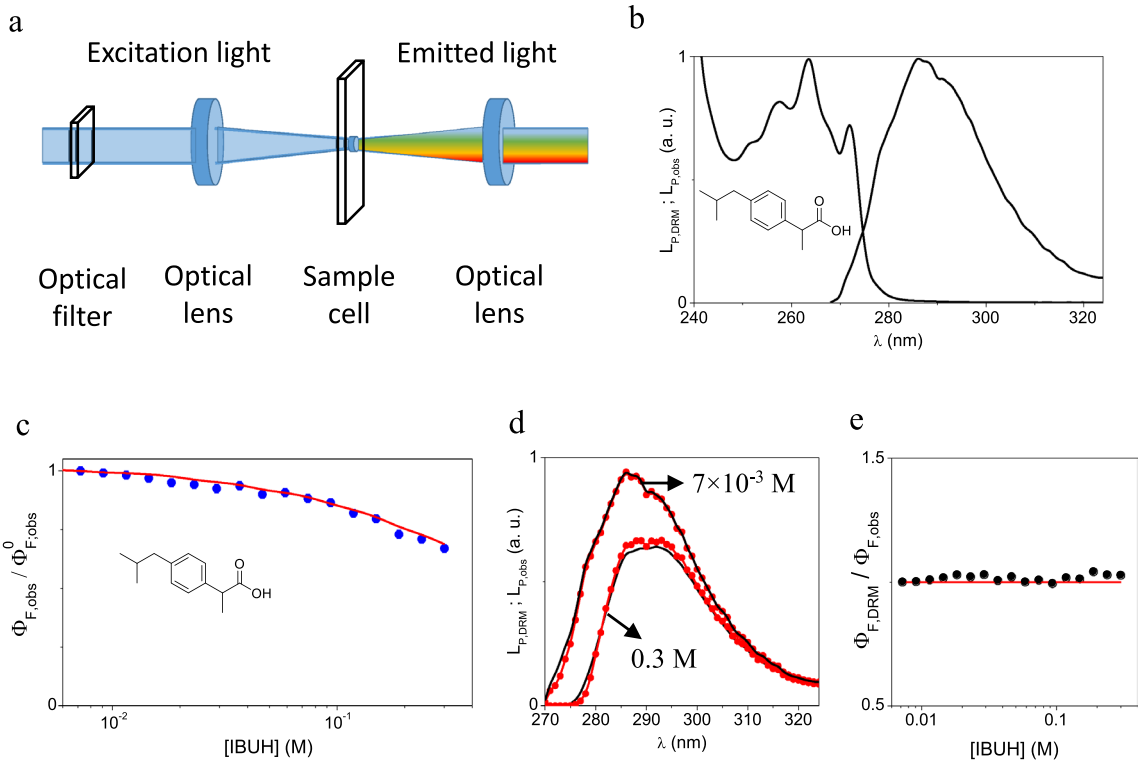

Fig. 1 **a** Scheme of the back-face transmission configuration used for fluorescence acquisition. **b** Normalized absorption and emission spectra of a 7×10^{-3} M ethanolic solution of HIbu. **c** Observed (blue dots) and DRM calculated (red line) fluorescence quantum yields of HIbu in ethanol, relative to diluted conditions, as a function of concentration. **d** Observed (black lines) and DRM calculated (red line and dots) fluorescence spectra of two ethanolic HIbu solutions: 7×10^{-3} and 0.3 M. **e** Stern–Volmer plot for the observed (black dots) and the calculated data (red line), the last one assuming $\Phi_{F,obs} = \Phi^0_{F,obs}$

re-absorption phenomena. Furthermore, the experimental fluorescence spectra are accurately reproduced by the DRM as observed in Fig. 1d. The invariance of the molecular fluorescence quantum yield of the probe as the concentration increases is also confirmed in the Fig. 1e, in which a Stern–Volmer graph—obtained by plotting $\Phi_{F,DRM}/\Phi_{F,obs}$ as a function of the concentration—shows a zero slope. These results, in addition to the invariance in the shape of the absorption spectra with the concentration (data not shown) strongly support the absence of molecular aggregation in the system, at least from a spectroscopic point of view.

2.2 Sodium ibuprofenate in aqueous solution

NaIbu in water shows a different behavior than HIbu in ethanol. Figure 2a shows that $\Phi_{F,obs} > \Phi_{F,DRM}$ for concentrations higher than 0.18 M, a value previously reported as the critical aggregation concentration (CAC) by other authors [17]. This observation indicates that a phenomenon different from reabsorption is present in the system above this concentration. To evaluate the origin of this enhanced fluorescence signal, some aspects must be discussed: (a) the detection of the re-emitted light could be considered in principle negligible, due to the low excitation and collection volumes used for the measurements; (b) the presence of scattering light and the eventual detection of emission coming from ground-state dimers and excimers could be discarded if the shape of the absorption and fluorescence spectra do not change with concentration. A careful inspection of the Fig. 2b reveals a slight increment of the intensity at the red side of the fluorescence spectra of concentrated samples compared with the diluted ones. This minor change cannot be entirely reproduced by scaling the shape of the molecular spectra of the NaIbu using the Equation a.2 included in the supporting material. It may be caused by either re-emission or scattering or by excimer formation (ground-state dimers are discarded due to the invariance of the shape of the absorption spectra, data not shown) and, at this stage, it is not possible to assess the precise nature of this shifted signal. However, the difference between the experimental spectra of the concentrated solutions and the scaled molecular NaIbu spectrum is, at most, 3%, a magnitude which is of the same order of the uncertainties associated to the fluorescence quantum yield measurements. All these arguments lead to suggest that the major part of the increment of the fluorescence

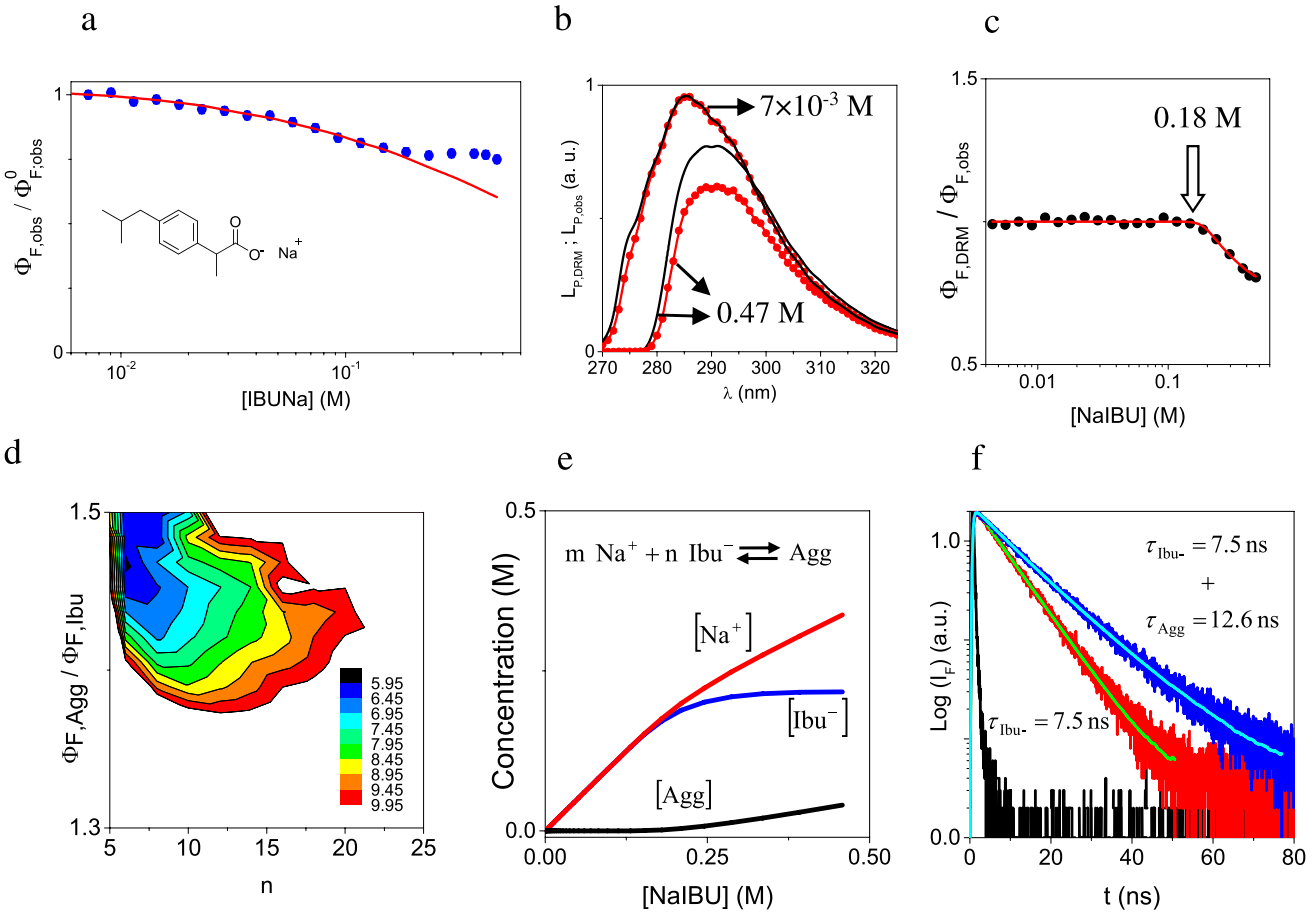

Fig. 2 **a** Observed (blue dots) and differential reabsorption model calculated (DRM, red line) fluorescence quantum yields relative to diluted conditions of NaIbu in water for different concentrations. **b** Observed (black line) and DRM calculated (red line and dots) fluorescence spectra of 7×10^{-3} and 0.47 M aqueous solutions of NaIbu. **c** Observed (black dots) and calculated using the closed association model (CAM, red line) Stern–Volmer plots. **d** χ^2 as a function of the Ibu^- aggregation number, n, and $\Phi_{F,Agg}/\Phi_{F,Ibu}$. **e** Equilibrium concentrations of Na^+ (red), Ibu^- (blue) and Agg (black) as a function of NaIbu concentration, calculated from CAM for $n=6$, $m=3$ and $K_{Agg}=10^4$. **f** Fluorescence decays ($\lambda_{ex}=260$ nm, $\lambda_{em}=290$ nm) of two different aqueous solutions of NaIbu: 7×10^{-3} M (red dots) and 0.42 M (blue dots). The black dots correspond to the instrument response function (IRF)

intensity after the CAC can be rationalized by assuming an enhancement in the molecular fluorescence quantum yield of Ibu^- when it takes part of the aggregates. In this respect, it was previously reported that the encapsulation of Ibu^- in cyclodextrins causes an enhancement in its fluorescence intensity due to a partial constrain of the isobutyl chain mobility [18].

The trend of the experimental data observed in Fig. 2c can be described by considering two different contributions to the total fluorescence as follows (see section c in the SM for details):

$$\frac{\Phi_{F,DRM}}{\Phi_{F,Obs}}=\left(\frac{[Ibu^-]}{C_0}\left(1-\frac{\Phi_{F,Agg}}{\Phi_{F,Ibu}}\right)+\frac{\Phi_{F,Agg}}{\Phi_{F,Ibu}}\right)^{-1} \quad (2)$$

where $\Phi_{F,ibu}$ and $\Phi_{F,Agg}$ are the molecular fluorescence quantum yield of the ibuprofenate anion free in solution and taking part of the aggregate, respectively, and $[Ibu^-]$ is the concentration of the ibuprofenate anion free in solution. The $[Ibu^-]$ was successfully obtained applying an iterative processes to solve the equations of the closed association model (CAM, see section b in the SM for details):

$$mX^+ + nIbu^- \rightleftarrows Agg \quad K_{Agg}=\frac{[Agg]}{[X^+]^m[Ibu^-]^n} \quad X^+=\{Na^+;BMIm^+\} \quad (3)$$

where m and n are the number of counterions and ibuprofenate anions that take part of the aggregate, respectively, $[X^+]$ is the counterion concentration, $[Agg]$ is the concentration of the aggregates of the form $X_mIbu_n^{(m-n)}$ and K_{Agg} is the aggregation constant. The model has four parameters to be adjusted: n, m,$\Phi_{F,Agg}/\Phi_{F,Ibu}$ and K_{Agg}. The results shown in Fig. 2c provide evidence of the accuracy of the model in reproducing the experimental data. The criterion used to

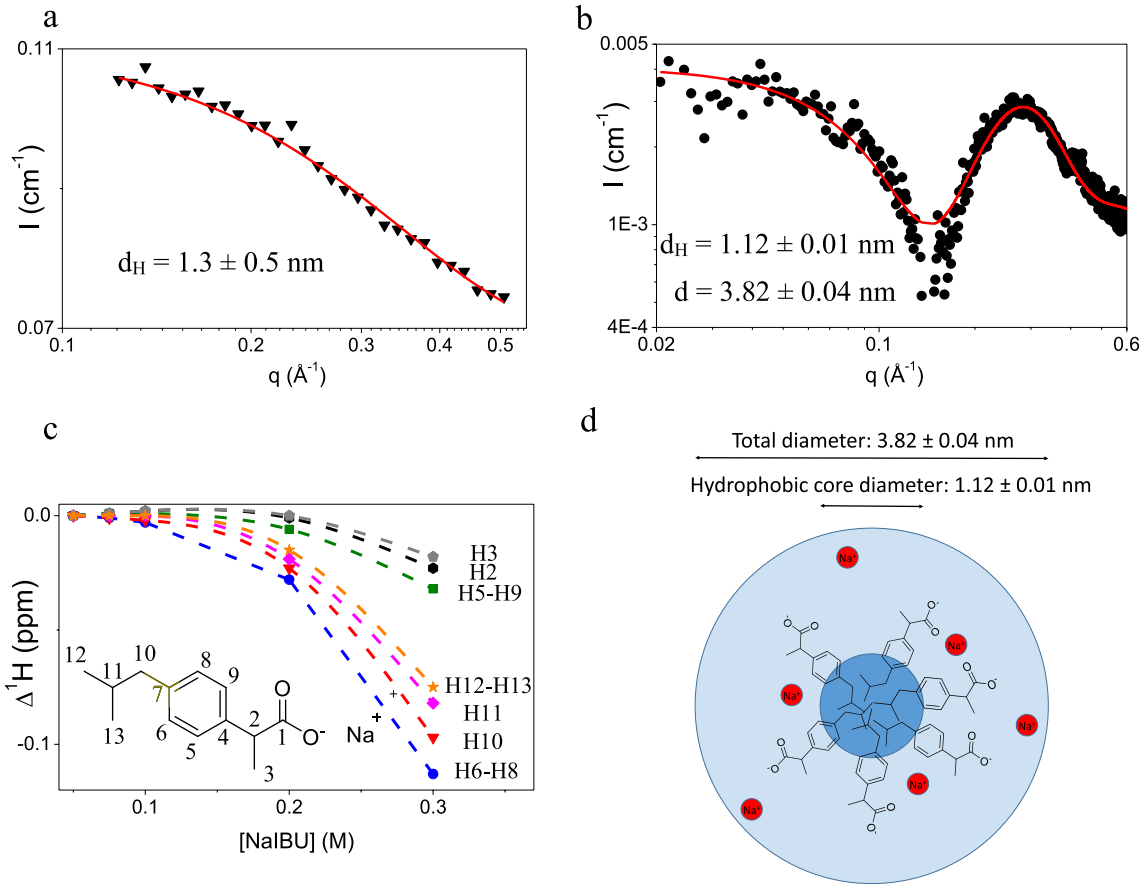

Fig. 3 **a** SANS pattern of a 0.2 M solution of NaIbu in D_2O (black triangles). The red solid line represents the Guinier-Porod model for spheres of hidrofobic diameter d_H of 1.3 ± 0.5 nm. **b** SAXS pattern of a 0.47 M aqueous solutions of NaIbu (black circles). The red solid line represents a core-shell model for spheres of hidrofobic diameter d_H of 1.12 ± 0.01 nm and an external diameter d of 3.82 ± 0.04 nm . **c** Variation of the ^{1}H-NMR signals of NaIbu in D_2O as a function of the concentration. **d** Scheme of the NaIbu aggregate

obtain the most acceptable fitting involves the minimization of the χ^2 parameter. As such, Fig. 2d shows that the values of n and $\Phi_{F,Agg}/\Phi_{F,Ibu}$ that minimize χ^2 are 6 and 1.46, respectively which, in turn, correspond to m = 3 and $K_{Agg} = 10^4$. The speciation diagram obtained with these parameters is presented in Fig. 2e. It is observed that [Ibu$^-$] remains fairly constant above the CAC value. Time-resolved experiments confirm the proposed interpretation. The fluorescence decay of NaIbu solutions below the CAC presents a mono-exponential behavior with $\tau_{Ibu}{}^- = 7.50 \pm 0.01$ ns, whereas above the CAC it shows a bi-exponential behavior with $\tau_{Ibu}{}^- = 7.4 \pm 0.4$ ns and $\tau_{Agg} = 12.6 \pm 0.2$ ns, as observed in Fig. 2f. This feature confirms that two different populations of emitting Ibu$^-$ in the system: one corresponding to the free monomer in solution and a second one to molecules forming part of the aggregates. In addition, the ratio $\tau_{Agg}/\tau_{Ibu}{}^- = 1.7 \pm 0.1$ agrees reasonably well with the value of 1.46 obtained for $\Phi_{F,Agg}/\Phi_{F,Ibu}$ from the modeling of the fluorescence steady-state data, supporting the idea of changes in the non-radiative constant of the fluorophore.

Although there is a minimum in χ^2 that serves to determine the four parameters of interest, the fitting can be described by the interval of parameter's values that comprise a χ^2 standard deviation: $n = (6–20)$, $\Phi_{F,Agg}/\Phi_{F,Ibu} = (1.37–1.50)$, $m = (3–13)$ and $K_{Agg} = (10^3–10^7)$. As such, although it is not possible to determine which set of parameters is better to describe the system, it is possible to rule out, with a certainty of 90%, a value of $n = 40$. This result contrasts with aggregation numbers previously reported of 40 [17], 44 [19], and 48 [20] by other authors for the same system. A possible source of the observed differences may be due to the fact that all these authors utilize external fluorescent probes for their determinations which, in turn, can cause changes in the aggregation number, as mentioned above.

To support the results obtained from direct fluorescence experiments, the aggregate entities in concentrated NaIbu solutions were also studied by nuclear magnetic resonance

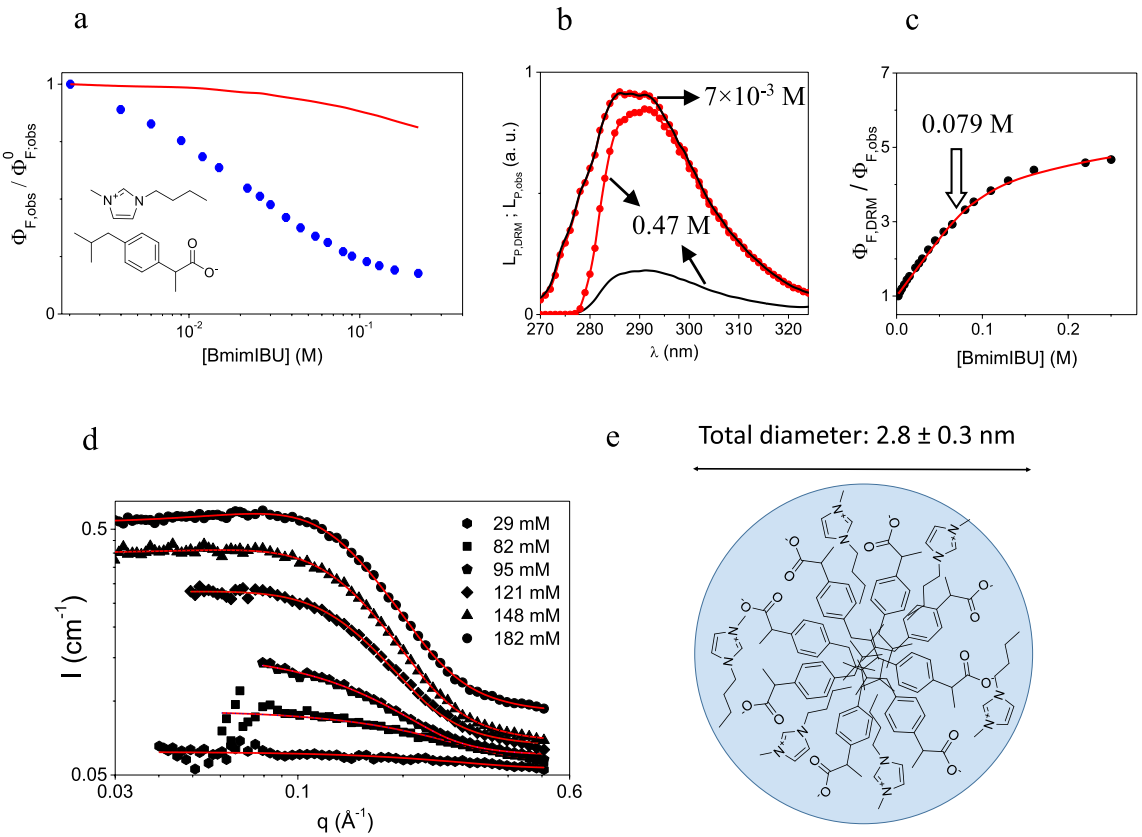

Fig. 4 **a** Observed (blue dots) and DRM-calculated (red line) $\Phi_{F,obs}/\Phi^{0}_{F,obs}$, for BMImIbu in water as a function of concentration. **b** Observed (black line) and DRM-calculated (red line and dots) fluorescence spectra of 2×10^{-3} and 0.30 M. **c** Observed (black dots) and calculated using the CAM for aggregation (red line) Stern–Volmer plots. **d** SANS patterns of BMImIbu in D_2O for different concentrations. **e** Scheme of the BMImIbu aggregate

(NMR) and small-angle neutron and X-ray scattering (SANS and SAXS, respectively). Figure 3a shows the SANS pattern of a 0.2 M solution of NaIbu in D_2O. The results reveal the presence of spherical objects of 1.3 ± 0.5 nm of diameter attributed to the aggregation of ca. 7 hydrophobic tails of ibuprofenate anions. In contrast, Fig. 3b shows the SAXS pattern of a 0.47 M solution of NaIbu in water that is compatible with a core–shell-like object with a spherical center of 1.12 ± 0.01 nm of diameter (hydrophobic center) and an external spherical region of 1.35 ± 0.01 nm of thickness corresponding to hydrophilic heads and counterions (see section d in the SM for details). Figure 3c shows that the most affected ^{1}H-NMR signals at higher concentrations are those corresponding to the hydrogen atoms of the isobutyl chain (see section e in the SM for details). This result supports the hypothesis of the presence of a hydrophobic center in which the isobutyl chain mobility is restricted. In addition, it also reinforces the hypothesis of the de-activation of the non-radiative pathway associated with the isobutyl chain mobility which, in turn, would explain the enhancement of the molecular Φ_F and the τ of the probe when it takes part of the aggregate. Figure 3d shows a schematic representation of the NaIbu aggregates that encompasses all these results.

2.3 1-Butyl-3-methylimidazolium ibuprofenate in aqueous solution

The last system examined comprises BMimIbu in water. Figure 4a shows a marked decrease of Φ_F as the concentration of BMimIbu increases that cannot be explained by re-absorption. The quenching of ibuprofenate fluorescence in this case is caused by the imidazolium cations, as previously reported for similar systems [21]. Figure 4b shows that the quenching phenomenon proceeds without changes in the shape of the emission spectrum. The Stern–Volmer plot (Fig. 4c) shows an almost linear behavior of $\Phi_{F,DRM}/\Phi_{F,obs}$ at lower concentrations reaching a plateau at higher concentrations. These results can be accurately described by a model that assumes that the fluorescence of Ibu^- is totally quenched by $BMim^+$ in the aggregates and is collisional quenched by the same species in solution, according to:

$$\frac{\Phi_{F,DRM}}{\Phi_{F,Obs}} = 1 + k_{SV} \cdot [BMim^+], \quad (4)$$

where the $BMim^+$ concentration in solution was obtained from the CAM (Eq. 3) by an iterative process (see section c in the SM for details). The model has also four parameters to be adjusted: n, m, K_{Agg} and k_{SV}. The optimized values obtained are: $n = 8$, $m = 6$, $K_{Agg} = 6 \times 10^{12}$ and $k_{SV} = 31.4\ M^{-1}$. Considering a fluorescence lifetime for Ibu^- in water of 7.5 ns, the quenching constant $k_q = \frac{k_{SV}}{\tau} \sim 4 \times 10^9\ M^{-1}\ s^{-1}$ would suggest a diffusional process in water solution. SANS patterns (Fig. 4d) evidence the presence of spherical objects of 2.8 ± 0.3 nm of diameter in solutions of BMImIbu above the CAC of 0.075 M [13]. The number of these objects increases with concentration although their size remains similar, at least for the concentration range studied. The volume of the aggregate entities is in good agreement with the aggregation numbers calculated from the CAM and those previously reported from molecular dynamics simulations [22]. Figure 4e shows a schematic representation of the BMImIbu aggregates. The interaction of the isobutyl chains is supported by the ^{1}H-NMR spectra provided previously [22], which are quite similar to that reported for NaIbu.

3 Conclusions

This study demonstrates that the back-face transmission steady-state fluorescence acquisition is a promising strategy to study the aggregation process of fluorescent amphiphilic molecules with low aggregation number and high CAC values. There are few examples in literature focused on the use of front-face geometry to determine the CMC of some non-ionic fluorescent surfactants such as Triton X-100, Triton X-114, and TritonX-165 [23, 24]. However, the CMC values of such compounds are lower than 1 μM for which the absorbance is not so high and the effects of re-absorption on the fluorescence spectra are minimal. The strategy presented, although limited to fluorescent molecules, allows the characterization of the aggregation of amphiphilic molecules without the need of external probes.

Supplementary Information The online version contains supplementary material available at https://doi.org/10.1007/s43630-022-00247-7.

Acknowledgements P.Y.S. has a postdoctoral fellowship from CONICET. N.I.K. is a staff member of CNEA. G.P.S. had a postdoctoral fellowship from CNEA. D.R., C. H-I. and A. Z. are staff members of CONICET. D.C. is a staff member of HZB. M.M. is a staff member of CNEA and CONICET. The authors thank María Laura Japas and Hugo Bianchi for the efforts made to obtain the optical filters, and Daniel Laria for further discussion of the manuscript.

Author contributions GPS and NIK synthesized, purified and characterized the NaIbu and the BMimIbu. GPS, NIK and DR performed the steady-state fluorescence measurements. PYS and MM acquired the time-resolved decays. PYS and DC performed the SANS measurements. CH-I performed the SAXS measurements. PYS and CH-I implemented the SANS and SAXS analysis. AZ and MM carried out the analysis of fluorescence data. DR contributed to the statistical analysis. All authors contributed to the discussion of the results. PYS, AZ and MM wrote the manuscript.

Funding M.M., D.R., P.Y.S. and N.I.K. received funding from ANPCyT (PICT2019-02034). M.M., P.Y.S. and N.I.K. received funding from ANPCyT (PICT2019-01615).D.R., M.M. and N.I.K. received funding from ANPCyT (PICT2018-02153). P.Y.S. received a fellowship from IAEA (EVT1901584-0001-ARG).

Declarations

Conflict of interest On behalf of all authors, the corresponding author states that there is no conflict of interest.

References

1. Mukherjee, I., Moulik, S. P., & Rakshit, A. K. (2013). Tensiometric determination of Gibbs surface excess and micelle point: A critical revisit. *Journal of Colloid & Interface Science, 394*, 329–336.
2. Marcolongo, J. P., & Mirenda, M. (2011). Thermodynamics of sodium dodecyl sulfate (SDS) micellization: An undergraduate laboratory experiment. *Journal of Chemical Education, 88*, 629–633.
3. Patist, A., Bhagwat, S. S., Penfield, K. W., Aikens, P., & Shah, D. O. (2000). On the measurement of critical micelle concentrations of pure and technical-grade nonionic surfactants. *Journal of Surfactants Detergents, 3*, 53–58.
4. Fluksman, A., & Benny, O. (2019). A robust method for critical micelle concentration determination using cumarin-6 as a fluorescent probe. *Analytical Methods, 11*, 3810–3818.
5. Pernak, J., & Skrzypczak, A. (1996). 3-Alkylthiomethyl-l-ethylimidazolium chlorides. Correlation between critical micelle concentrations and minimum inhibitory concentrations. *European Journal of Medicinal Chemistry, 31*, 901–903.
6. Ottaviani, G., Wendelspiess, S., & Alvarez-Sanchez, R. (2015). The importance of critical micellar concentration for the prediction of solubility enhancement in biorelevant media. *Molecular Pharmaceutics, 12*, 1171–1179.
7. Su, H., Wang, F., Ran, W., Zhang, W., Dai, W., Wang, H., Anderson, C. F., Wang, Z., Zheng, C., Zhang, P., Li, Y., & Cui, H. (2020). The role of critical micellization concentration in efficacy and toxicity of supramolecular polymers. *Proceedings of the National Academic of Science USA, 117*, 4518–4526.
8. Fujii, S., Yamada, S., Matsumoto, S., Kubo, G., Yoshida, K., Tabata, E., Miyake, R., Sanada, Y., Akiba, I., Okobira, T., Yagi, N., Mylonas, E., Ohta, N., Sekiguchi, H., & Sakurai, K. (2017). Platonic micelles: Monodisperse micelles with discrete aggregation numbers corresponding to regular polyhedra. *Scientific Reports, 7*, 44494.
9. Kalyanasundaram, K., & Thomas, J. K. (1977). Environmental effects on vibronic band intensities in Pyrene monomer fluorescence and their application in studies of micellar systems. *Journal of American Chemical Society, 99*, 2039–2044.
10. Aguiar, J., Carpena, P., Molina-Bolívar, J. A., & Carnero-Ruiz, C. (2003). On the determination of the critical micelle concentration by the Pyrene 1:3 ratio method. *Journal of Colloid & Interface Science, 258*, 116–122.

11. Turro, N. J., & Yekta, A. (1978). Luminescent probes for detergent solutions. A simple procedure for determination of the mean aggregation number of micelles. *Journal of American Chemical Society, 100*, 5951–5952.
12. García, N. H., Porta, D. J., Alasino, R. V., Muñoz, S. E., & Beltramo, D. M. (2020). Ibuprofen, a traditional drug that may impact the course of COVID-19. New effective formulation in nebulizable solution. *Medical Hypotheses, 144*, 110079.
13. Tourné-Péteilh, C., Devoisselle, J.-M., Vioux, A., Judeinstein, P., In, M., & Viau, L. (2011). Surfactant properties of ionic liquids containing short alkyl chain imidazolium cations and ibuprofenate anions. *Physical Chemistry Chemical Physics, 13*, 15523–15529.
14. Rodrigues, D., Sarmiento, G. P., Krimer, N. I., & Mirenda, M. (2020). Radioluminescent ionic liquids: Designer materials for detecting and quantifying ionizing radiation. *ACS Applied Electronic Materials, 2*, 2662–2668.
15. Krimer, N. I., Rodrigues, D., Rodríguez, H. B., & Mirenda, M. (2017). Steady-state fluorescence of highly absorbing samples in transmission geometry: A simplified quantitative approach considering reabsorption events. *Analytical Chemistry, 89*, 640–647.
16. Rodríguez, H. B., Mirenda, M., Lagorio, M. G., & San Román, E. (2019). Photophysics at unusually high dye concentrations. *Accounts of Chemical Research, 52*, 110–118.
17. Ridell, A., Evertsson, H., Nilsson, S., & Sundelöf, L.-O. (1999). Amphiphilic association of ibuprofen and two nonionic cellulose derivatives in aqueous solution. *Journal of Pharmacological Sciences, 88*, 1175–1181.
18. Oh, I., Lee, M.-Y., Lee, Y.-B., Shin, S.-C., & Park, H. (1998). Spectroscopic characterization of ibuprofen/2-hydroxypropyl-β-cyclodextrin inclusion complex. *International Journal of Pharmcology, 175*, 215–223.
19. Azuma, N., Ahmed, A., Rub, M. A., Asiri, A. M., & Alamery, S. F. (2019). Investigation of sggregation behavior of ibuprofen sodium drug under the influence of gelatin protein and salt. *Journal of Molecular Liquids, 290*, 111187.
20. Dey, A., Sandre, V., Marangoni, D. G., & Ghosh, S. (2018). The interaction between a non-steroidal anti-inflammatory drug (Ibuprofen) and anionic surfactant AOT and effect of salt (NaI) and hydrotrope (4-4-4). *Journal of Physical Chemistry B, 122*, 3974–3987.
21. Sanan, R., Kaur, R., & Mahajan, R. K. (2014). Micellar transitions in catanionic ionic liquid–ibuprofen aqueous mixtures; effects of composition and dilution. *RSC Advances, 4*, 64877–64889.
22. Tourné-Péteilh, C., Coasne, B., In, M., Brevet, D., Devoisselle, J.-M., Vioux, A., & Viau, L. (2014). Surfactant behavior of ionic liquids involving a drug: From molecular interactions to self-assembly. *Langmuir, 30*, 1229–1238.
23. Anand, U., Jash, C., & Mukherjee, S. (2011). Spectroscopic determination of critical micelle concentration in aqueous and non-aqueous media using a non-invasive method. *Journal of Colloid & Interface Science, 364*, 400–406.
24. Jaiswal, S., Mondal, R., Paul, D., & Mukherjee, S. (2016). Investigating the micellization of the triton-X surfactants: A non-invasive fluorometric and calorimetric approach. *Chemical Physics Letters, 646*, 18–24.

Authors and Affiliations

Paula Y. Steinberg[1] · Nicolás I. Krimer[1] · Gabriela P. Sarmiento[1] · Darío Rodrigues[1,2] · Cristián Huck-Iriart[3] · Daniel Clemens[4] · Andrés Zelcer[5] · Martín Mirenda[1]

✉ Martín Mirenda
mirenda@cnea.gov.ar

[1] Gerencia Química, Centro Atómico Constituyentes, Comisión Nacional de Energía Atómica (CNEA-CONICET), Av. Gral. Paz 1499, San Martín, B1650KNA Buenos Aires, Argentina

[2] Departamento de Física, Facultad de Ciencias Exactas y Naturales, Universidad de Buenos Aires (UBA-CONICET), Ciudad Universitaria, Pab. I, C1428EHA Buenos Aires, Argentina

[3] Instituto de Tecnologías Emergentes y Ciencias Aplicadas (ITECA), UNSAM-CONICET, Escuela de Ciencia y Tecnología, Laboratorio de Cristalografía Aplicada, Campus Miguelete, 25 de Mayo y Francia, 1650 San Martín, Buenos Aires, Argentina

[4] Helmholtz-Zentrum Berlin, Hahn-Meitner-Platz 1, 14109 Berlin, Germany

[5] CIBION, CONICET, Godoy Cruz 2390, C1425FQD Buenos Aires, Argentina